Advances in Nano Research, *Vol. 15, No. 3 (2023) 191-201*
https://doi.org/10.12989/anr.2023.15.3.191

Investigation on the heat transfer of MHD nanofluids in channel containing porous medium using lattice Boltzmann method

Xiangyang Liu, Jimin Xu, Tianwang Lai and Maogang He*

Key Laboratory of Thermal Fluid Science and Engineering of MOE, School of Energy and Power Engineering, Xi'an Jiaotong University, No.28, Xianning West Road, Xi'an, Shaanxi, 710049, P.R. China

(*Received July 13, 2021, Revised June 9, 2023, Accepted June 13, 2023*)

Abstract. In order to develop better method to enhance and control the flow and heat transfer inside the radiator of electronic device, the synergistic effect of MHD nanofluids and porous medium on the flow and heat transfer in rectangular opened channel is simulated using Lattice Boltzmann method. Three nanofluids of CuO-water, Al_2O_3-water and Fe_3O_4-water are studied to analyze the influence of the type of nanofluid on the synergistic effect. The simulation results show that the porous medium can increase the flow velocity in fluid zone adjacent to the porous medium and enhance the heat transfer on the surface of the channel. Under no magnetic field, when the porosity of porous medium is 0.8, the Nusselt number is 4.46% higher than when the porosity is 0.9. Al_2O_3-water has the best heat transfer effect among the three nanofluids. At Φ=0.06, *Ha*=100, θ=90°, ε=0.9, *Nu* of Al_2O_3-water is 6.51% larger than that of CuO-water and 5.05% larger than that of Fe_3O_4-water. Magnetic field enhances seepage in porous medium and inhibits heat transfer in the bottom wall. When *Ha*=30 and 60, the inhibiting effect is the most significant as the magnetic field angle is 90°. And when *Ha*=100, the inhibiting effect is the most significant as the magnetic field angle is 120°.

Keywords: heat transfer; LBM; MHD; nanofluid; porous medium

1. Introduction

The characteristics of small size and high power of modern electronic devices make highly-efficient heat dissipation technology much important (Mondal *et al*. 2016, Babar and Ali 2019, Khan *et al*. 2020). Nanofluid which is a fluid containing suspended nanoparticles with 100 nm diameter or smaller (Darbari *et al*. 2020, Dai *et al*. 2021, Mebarek-Oudina and Chabani 2022) has been widely studied as one method to enhance heat transfer (Habibzadeh *et al*. 2010, Patel *et al*. 2003, Yu *et al*. 2004). It can be used as heat exchangers especially in electronic devices and heat sink with microchannel (Mebarek-Oudina 2018). The heat transfer effect of nanofluids depend on the properties of nanoparticles and base fluid as well as the dispersion of nanoparticles (Cardellini *et al*. 2016, Iqbal *et al*. 2021). Krishna *et al*. studied the heat transfer of Al_2O_3-H_2O and TiO_2-H_2O nanofluids in a rectangular microchannel heat exchanger, and found that Al_2O_3-H_2O and TiO_2-H_2O nanofluids can significantly improve the heat dissipation of electronic equipment (Murali Krishna and Sandeep Kumar 2019). Singh *et al*. (2021) synthesized Fe_2O_3-ethylene glycol nanofluid and found the thermal conductivity of ethylene glycol can be significantly improved by loading a very low concentration of nanoparticle, which indicates that this nanofluid has potential application in heat transfer management of electronic devices.

Nanofluids are usually conducting fluids, and their behaviors under the action of magnetic fields are different from non-conducting fluids (Boujelbene *et al*. 2023, Shafiq *et al*. 2022). Magnetic field can induce current in flowing conductive fluid, thereby exerting a Lorentz force on the fluid (Ramesh *et al*. 2023, Mebarek-Oudina *et al*. 2023). Magnetic field is a potential technology to control heat transfer process in devices by regulating the flow process of nanofluids through the Magnetohydrodynamic (MHD) force (Manna *et al*. 2021, Sheikholeslami *et al*. 2014, Beriache *et al*. 2016). Ma *et al*. (2020) found that parallel magnetic fields could enhance the natural convection heat transfer of Fe_3O_4-water nanofluids, due to the influence on the convective energy transport. And with the increase of the number of nanoparticles, the average Nusselt number (*Nu*) increases linearly. Sharif *et al*. (2021a) analyzed the biological convection phenomenon in the MHD boundary layer flow of Powell-Eyring nanofluid through a stretchable cylinder with Cattaneo-Christov heat flux. The results show that the concentration of nanofluid increases with the magnetic field parameter, which enhances the local heat transfer). Farooq *et al*. simulated the MHD flow of SiO_2/MoS_2-propylene glycol nanofluids over a stretched surface. It was found that as the magnetic parameter increased, the fluids speed decreased, and the heat dissipation became worse (Farooq *et al*. 2023). Khan *et al*. investigated the effect of Lorentz force on the Casson fluid flow of water-based Fe_3O_4-MWCNT hybrid nanofluid induced by dust particles from a stretched sheet. It is found that magnetic field can inhibit the fluid flow. (Khan *et al*. 2022).

In some applications, the insertion of porous medium in nanofluid-filled cavities can improve the overall heat transfer efficiency. The porous medium dissipates the

*Corresponding author, Professor
E-mail: mghe@mail.xjtu.edu.cn

ISSN: 2287-237X (Print), 2287-2388 (Online)

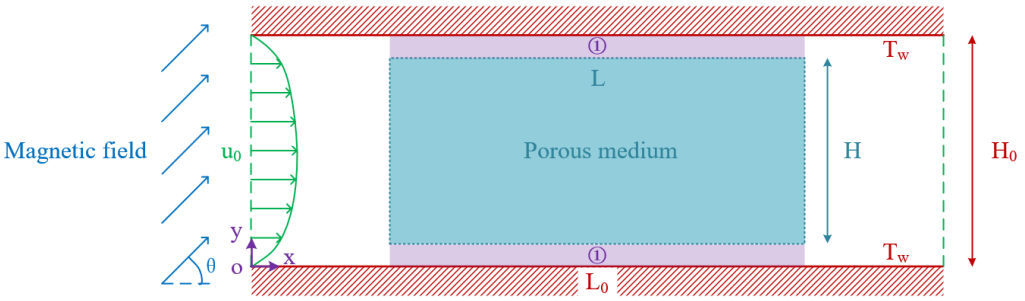

Fig. 1 Schematic diagram of the problem

kinetic energy of the flow and reduces the convective heat transfer. However, the heat conduction of the porous media compensates for the loss, thereby enhancing the heat transfer (Kadhim *et al*. 2023). Therefore, some scholars combined porous medium with MHD nanofluids to enhance the flow and heat transfer process. Sajjadi *et al*. (2019) used a novel dual multiple relaxation time (MRT) lattice Boltzmann method (LBM) to simulate the MHD natural convection of MWCNT-Fe_3O_4/water hybrid nanofluids in porous medium. The results show that increasing the magnetic field parameter suppresses the natural convection. The larger porosity of the porous medium, the greater heat transfer. Sheikholeslami *et al*. (2019) studied the forced non-Darcy percolation of Al_2O_3-water nanofluids in a three-dimensional ellipsoidal heater with porous medium under a uniform magnetic field. It is shown that increase in permeability of porous medium will enhance intensity of heat plume, and the magnetic field will inhibit the convection. Li *et al*. (2019) simulated Lorentz force effect on the heat transfer process of the nanofluid which flows through the permeable tube. In Li's model, Nusselt number increases with the increasing of permeability of porous medium and strength of the magnetic field. Rao and Deka investigated the stable, incompressible MHD flow of SWCNT/Al_2O_3-water hybrid nanofluid over a vertical solid cone embedded in a porous medium under suction. It is found that the temperature in the boundary layer region increases with the increase of magnetic field and porosity (Rao and Deka 2023).

From the above, it is clear that studies on the flow and heat transfer of MHD nanofluids in porous medium are usually proposed for scenarios with practical applications. However, the heat dissipation problems of electronic devices mentioned in this paper often require small volume planar heat dissipation, such as heat dissipation for chips, circuit boards, and hot ends of thermoelectric coolers. This requires flat and forced convection of the liquid cooling channels for planar heat dissipation. Unfortunately, this has not been studied in previous research.

In order to achieve planar heat dissipation for electronic devices, this paper simulates the flow and heat transfer of MHD nanofluid in a flow channel filled with porous medium. The simulation method uses LBM with MRT forma on the representative elementary volume (REV) scale. Because metal oxide nanoparticles are abundant and cheap. At the same time, CuO, Al_2O_3 and Fe_3O_4 nanoparticles play a key role in improving the thermal conductivity of traditional fluids (Nfawa *et al*. 2021, Yusoff *et al*. 2018). This paper selects these three nanoparticles with different concentration as the working fluids. To characterize effect of porous medium on flow and heat transfer, the porosity will be varied from 0.8 to 0.95. The effect of magnetic field will be considered in terms of magnetic field strength and direction.

2. Problem statement

The forced flow of nanofluid in the rectangular opened channel was studied by using the lattice Boltzmann model of D_2Q_9. The schematic diagram of the problem is shown in Fig.1.

The upper and lower wall are at a fixed temperature T_w. The aspect ratio of the channel equals to 3 (L_0/H_0=3). There is a porous medium with the length of $0.6L_0$ and the width of $0.8H_0$ filled in the center of the channel. The dimensionless specific surface area S_y of porous medium is 40. The full developed flow of nanofluid enters the channel with a parabolic velocity profile and the average flow rate is u_0. The flow process is regarded as incompressible laminar Newtonian flow. CuO-water, Al_2O_3-water and Fe_3O_4-water nanofluids were studied in this work. A uniform magnetic field at direction θ with a magnetic induction intensity of $\vec{B}$ is applied in the channel. $\vec{B}$ is defined as:

$$\vec{B} = B_x\vec{e_x} + B_y\vec{e_y} \tag{1}$$

$$tan\,\theta = \frac{B_y}{B_x} \tag{2}$$

where $\vec{e_x}$ and $\vec{e_y}$ are the unit vectors in the x and y directions, B_x and B_y are the magnetic-field strengths in the x and y directions. The electric current $\vec{J}$ and the electromagnetic force $\vec{F_e}$ are defined as:

$$\vec{J} = \sigma\left(\vec{V} \times \vec{B}\right) \tag{3}$$

$$\vec{F_e} = \sigma\left(\vec{V} \times \vec{B}\right) \times \vec{B} \tag{4}$$

where, $\vec{V}$ is velocity, σ is conductivity. The change of magnetic field strength is represented by the change of Hartmann number *Ha*. The thermophysical properties of water and nanoparticles are listed in Table 1.

Assuming that the nanoparticle and the base fluid are in thermal equilibrium, and the difference in the temperature

Table 1 Thermo-physical properties of different nano-particles and base liquid (see, Khan *et al*. 2020, Ellahi *et al*. 2018, Krishanan *et al*. 2020)

	k(W/m·K)	c_p(J/kg·K)	ρ(kg/m^3)	μ(Pa·s)	σ(Ω·m)$^{-1}$
Water (Li *et al*. 2019)	0.613	4179.8	995.65	7.97×10^{-4}	5.0×10^{-2}
CuO (Li *et al*. 2019)	18	540.0	6500.00	-	2.7×10^{-8}
Al_2O_3 (Sheikholeslami *et al*. 2016)	40	765.0	3970.00	-	1.0×10^{-10}
Fe_3O_4 (Abedini *et al*. 2019)	6	670.0	5200.00	-	2.5×10^{4}

and velocity between the two phases, the induced magnetic field generated by the motion of the conductive fluid, the Joule heating and viscous dissipation effects can be ignored, the continuity equation, momentum equation and energy equation are expressed as follows:

$$\frac{\partial u_x}{\partial x}+\frac{\partial u_y}{\partial y}=0 \tag{5}$$

$$\rho\left(u_x\frac{\partial u_x}{\partial x}+u_y\frac{\partial u_x}{\partial y}\right)=-\frac{\partial p}{\partial x}+\mu_{nf}\left(\frac{\partial^2 u_x}{\partial x^2}+\frac{\partial^2 u_x}{\partial y^2}\right) \\ -\sigma B^2\left(u_x\sin^2\theta-u_y\sin\theta\cos\theta\right)-\frac{\varepsilon\nu}{K}u_x-\frac{\varepsilon F_e}{\sqrt{K}}uu_x \tag{6}$$

$$\rho\left(u_x\frac{\partial u_y}{\partial x}+u_y\frac{\partial u_y}{\partial y}\right)=-\frac{\partial p}{\partial y}+\mu_{nf}\left(\frac{\partial^2 u_y}{\partial x^2}+\frac{\partial^2 u_y}{\partial y^2}\right) \\ -\sigma B^2\left(u_y\cos^2\theta-u_x\sin\theta\cos\theta\right)-\frac{\varepsilon\nu}{K}u_y-\frac{\varepsilon F_e}{\sqrt{K}}uu_y \tag{7}$$

$$u_x\frac{\partial T}{\partial x}+u_y\frac{\partial T}{\partial y}=\alpha_{nf}\left[\frac{\partial^2 T}{\partial x^2}+\frac{\partial^2 T}{\partial y^2}\right] \tag{8}$$

3. Parameter calculation

The density ρ_{nf}, heat capacity $(\rho c_p)_{nf}$, and electrical conductivity σ_{nf} of nanofluid can be calculated by (Izadi *et al*. 2018):

$$\rho_{nf}=(1-\phi)\rho_f+\phi\rho_s \tag{9}$$

$$\left(\rho c_p\right)_{nf}=(1-\phi)\left(\rho c_p\right)_f+\phi\left(\rho c_p\right)_s \tag{10}$$

$$\frac{\sigma_{nf}}{\sigma_f}=1+\frac{3\left(\frac{\sigma_s}{\sigma_f}-1\right)\phi}{\left(\frac{\sigma_s}{\sigma_f}+2\right)-\left(\frac{\sigma_s}{\sigma_f}-1\right)\phi} \tag{11}$$

where ρ, (ρc_p) and σ are the density, heat capacity and electrical conductivity, subscripts f and s stand for fluid and nanoparticle. Φ is the nanofluid volume fraction. Thermal conductivity of nanofluid can be determined by using Hamilton-Crosser as following (Hamilton 1962):

$$\frac{k_{nf}}{k_f}=\left(\frac{k_s+(n-1)k_f+(n-1)\phi\left(k_f-k_s\right)}{k_s+(n-1)k_f+\phi\left(k_f-k_s\right)}\right) \tag{12}$$

$$n=\frac{3}{\psi},\qquad 0.5<n<6 \tag{13}$$

where k_{nf}, k_f and k_s are thermal conductivities of nanofluid, base fluid and nanoparticle, respectively; n is experimental form factor, and ψ is ratio of some volume sphere surface fraction to particle's surface. For spherical particles, ψ=1.

Assuming that the nanoparticles are spherical, the viscosity of the nanofluid can be calculated by Brinkman relation (Brinkman 1952):

$$\mu_{nf}=\frac{\mu_f}{(1-\phi)^{2.5}} \tag{14}$$

$$\nu_{nf}=\frac{\mu_{nf}}{\rho_{nf}} \tag{15}$$

where μ_{nf} and ν_{nf} are the dynamic and kinematic viscosities of nanofluid, μ_f is the dynamic viscosity of the base fluid. *Ha* is defined as

$$Ha=B_0H_0\sqrt{\frac{\sigma_{nf}}{\rho_{nf}\nu_{nf}}} \tag{16}$$

Local *Nu* at the surface of bottom wall is defined as (Raza *et al*. 2022)

$$Nu_{loc}=-\frac{k_{nf}}{k_f}\frac{\partial T}{\partial n} \tag{17}$$

Average *Nu* at the surface of bottom wall is defined as

$$Nu_{avg}=\frac{1}{L_0}\int_0^{L_0}Nu_{loc}\,dx|_{y=0} \tag{18}$$

Relative average flow velocity in the x direction in fluid zone adjacent to porous medium (the location is shown as ① in Fig. 1) is defined as

$$\overline{U_x}=\frac{\overline{u_x}}{u_0} \tag{19}$$

where $\overline{u_x}$ is the average flow velocity in the x direction of zone ①.

4. Governing equations

4.1 Lattice Boltzmann method

4.1.1 Velocity field

The flow in the channel was simulated by using MRT-LBE model proposed by Guo and Zheng (Guo *et al*. 2008).

Compared with SRT-LBE, this format will make the computer iterative calculation more stable and have higher precision. The Boltzmann equation of this model is as follows:

$$f_i(\vec{x}+\vec{c_i}\delta_t, t+\delta_t) - f_i(\vec{x},t) = -(M^{-1}SM)_{ij}\left[f_i(\vec{x},t) - f_i^{(\mathrm{eq})}(\vec{x},t)\right] + \delta_t F_i \tag{20}$$

where f_i is density distribution function, $f_i^{(\mathrm{eq})}$ is density equilibrium distribution function, $\vec{x}$ means position vector, $\vec{c_i}$ means discrete lattice velocity in direction i, δ_t is lattice timestep, F_i is force term of porous medium, $\boldsymbol{M}$ is transformation matrix, $\boldsymbol{S}=diag(s_1,s_2,\ldots,s_b)$ is non-negative relaxation diagonal matrix. m_i and $m_i^{(\mathrm{eq})}$ represent momentum vector. The mapping of velocity and momentum space can be achieved by linear transformation:

$$m_i = Mf_i \tag{21}$$

$$m_i^{(\mathrm{eq})} = Mf_i^{(\mathrm{eq})} \tag{22}$$

The matrix $\boldsymbol{M}$ of the D_2Q_9 model is:

$$M = \begin{pmatrix} 1 & 1 & 1 & 1 & 1 & 1 & 1 & 1 & 1 \\ -4 & -1 & -1 & -1 & -1 & 2 & 2 & 2 & 2 \\ 4 & -2 & -2 & -2 & -2 & 1 & 1 & 1 & 1 \\ 0 & 1 & 0 & -1 & 0 & 1 & -1 & -1 & 1 \\ 0 & -2 & 0 & 2 & 0 & 1 & -1 & -1 & 1 \\ 0 & 0 & 1 & 0 & -1 & 1 & 1 & -1 & -1 \\ 0 & 0 & -2 & 0 & 2 & 1 & 1 & -1 & -1 \\ 0 & 1 & -1 & 1 & -1 & 0 & 0 & 0 & 0 \\ 0 & 0 & 0 & 0 & 0 & 1 & -1 & 1 & -1 \end{pmatrix} \tag{23}$$

The equilibrium momentum vector defined as:

$$m_i^{(\mathrm{eq})} = \rho\begin{pmatrix} 1, -2+3|\vec{u}|^2, 1-3|\vec{u}|^2, \\ u_x, -u_x, u_y, -u_y, u_x^2-u_y^2, u_xu_y \end{pmatrix}^T \tag{24}$$

where ρ is lattice fluid density; $\vec{u}$ is lattice fluid velocity; Besides, the force term of porous medium F_i is given by (Guo *et al*. 2002):

$$F_i = \omega_i\rho\left(1-\frac{1}{2\tau}\right)\left[\frac{\vec{c_i}\cdot\vec{F}}{{c_s}^2} + \frac{\vec{u}\vec{F}:(\vec{c_i}\vec{c_i}-{c_s}^2 I)}{\varepsilon {c_s}^4}\right] \tag{25}$$

where ω_i is weighting factor; c_s is lattice sound speed; τ is dimensionless lattice relaxation time for velocity; ε is porosity of porous medium; I represents unit tensor; $\vec{F}$ is external force on fluid. Considering the influence of magnetic field force and the resistance of porous medium, the external force $\vec{F}$ on the fluid is defined as:

$$\vec{F} = \vec{F}_x + \vec{F}_y \tag{26}$$

where $\vec{F}_x$ and $\vec{F}_y$ are the external force $\vec{F}$ in x and y directions, respectively.

For the nanofluid inside porous medium:

$$|\vec{F}_x| = -\frac{\varepsilon\nu}{K}u_x - \frac{\varepsilon F_\varepsilon}{\sqrt{K}}|\vec{u}|u_x + A\left(u_y \sin\theta\cos\theta - u_x\sin^2\theta\right) \tag{27}$$

$$|\vec{F}_y| = -\frac{\varepsilon\nu}{K}u_y - \frac{\varepsilon F_\varepsilon}{\sqrt{K}}|\vec{u}|u_y + A\left(u_x \sin\theta\cos\theta - u_y\cos^2\theta\right) \tag{28}$$

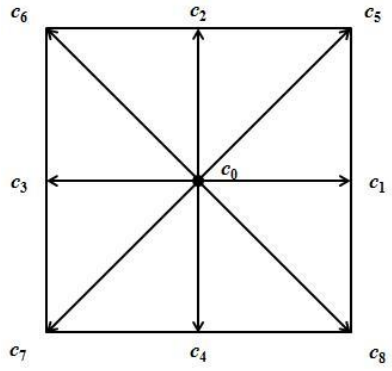

Fig. 2 Discrete velocity directions for D_2Q_9 model

where θ is direction of the uniform magnetic field, ν is viscosity of fluid; K is permeability of porous medium; F_ε is structure function.

For the nanofluid outside porous medium:

$$|\vec{F}_x| = A\left(u_y \sin\theta\cos\theta - u_x\sin^2\theta\right) \tag{29}$$

$$|\vec{F}_y| = A\left(u_x \sin\theta\cos\theta - u_y\cos^2\theta\right) \tag{30}$$

A is defined as:

$$A = \frac{Ha^2\mu}{H_0^{\ 2}} \tag{31}$$

F_ε and K can be calculated by Ergun empirical equation (Ergun 1952):

$$F_\varepsilon = \frac{1.75}{\sqrt{150}\varepsilon^{3/2}} \tag{32}$$

$$K = \frac{\varepsilon^3 {d_p}^2}{150(1-\varepsilon)^2} \tag{33}$$

where d_p is the average diameter of solid particles and can be calculated by:

$$d_p = \frac{2D(1-\varepsilon)}{SSA} \tag{34}$$

where D is dimension of the problem, i.e., D=2 for two-dimensional problem and D=3 for three-dimensional problem.

Where S_y is dimensionless specific surface area, which can be calculated by:

$$S_y = SSA \times H_0 \tag{35}$$

$$SSA = \frac{P}{HL} \tag{36}$$

where SSA is specific surface area of the porous medium, P is wet circumference of the porous medium, and L is the length of the porous medium.

As shown in Fig. 2, $\vec{c_i}$ for D_2Q_9 model is given by (Dong *et al*. 2018):

$$\vec{c_i} = \begin{cases} (0,0) i = 0 \\ c(cos[(i-1)\pi/2], sin[(i-1)\pi/2]) i = 1,2,3,4 \\ \sqrt{2}c(cos[(2i-1)\pi/4], sin[(2i-1)\pi/4]) i = 5,6,7,8 \end{cases} \tag{37}$$

where streaming speed is defined as $c=\delta x/\delta t$; δx and δt are lattice spacing and lattice timestep, respectively. Besides, weighting factor ω_i is expressed as (Kang *et al*. 2010):

$$\omega_i = \begin{cases} 4/9 i = 0 \\ 1/9 i = 1,2,3,4 \\ 1/36 i = 5,6,7,8 \end{cases} \quad (38)$$

c_s equals to $c/\sqrt{3}$.

Finally, ρ and $\vec{u}$ in porous medium is given by:

$$\rho = \sum_i f_i \quad (39)$$

$$\rho\vec{u} = \sum_i \vec{c_i} f_i + \frac{\delta_t}{2}\vec{F} \quad (40)$$

The modified rebound boundary format is used for the walls. This format has second-order precision. For example, at the upper wall boundary (He 2008):

$$f_{4,7,8}(i,m) = f_{2,5,6}(i,m) \quad (41)$$

where *m* means the lattice on upper boundary. The flow of the outlet is regarded as a fully developed flow. A fully developed boundary processing format is used to describe the export boundary conditions (He 2008):

$$f_{3,6,7}(n,j) = f_{3,6,7}(n-1,j) \quad (42)$$

where *n* means the lattice on outlet boundary. The velocity distribution at the inlet of the channel is parabolic, which is a known velocity boundary condition and is considered as (Mohamad 2015):

$$\rho_w = \frac{1}{1-u_{x,w}}[f_0 + f_2 + f_4 + 2(f_3 + f_6 + f_7)] \quad (43)$$

$$f_1 = f_3 + \frac{2}{3}\rho_w u_{x,w} \quad (44)$$

$$f_5 = f_7 - \frac{1}{2}(f_2 - f_4) + \frac{1}{6}\rho_w u_{x,w} + \frac{1}{2}\rho_w u_{y,w} \quad (45)$$

$$f_8 = f_6 + \frac{1}{2}(f_2 - f_4) + \frac{1}{6}\rho_w u_{x,w} - \frac{1}{2}\rho_w u_{y,w} \quad (46)$$

The boundary conditions at the four corners of the flow channel are defined as (Guo and Zheng 2008):

Northwest:

$$f_{1,4,8} = f_{3,2,6} \quad (47)$$

$$f_5 = \frac{1}{2}[\rho_0 - f_0 - 2(f_3 + f_2 + f_6)] \quad (48)$$

$$f_7 = f_5 \quad (49)$$

Southwest:

$$f_{1,2,5} = f_{3,4,7} \quad (50)$$

$$f_6 = \frac{1}{2}[\rho_0 - f_0 - 2(f_3 + f_4 + f_7)] \quad (51)$$

$$f_8 = f_6 \quad (52)$$

Northeast:

$$f_{3,4,7} = f_{1,2,5} \quad (53)$$

$$f_8 = \frac{1}{2}[\rho_0 - f_0 - 2(f_1 + f_2 + f_5)] \quad (54)$$

$$f_6 = f_8 \quad (55)$$

Southeast:

$$f_{3,2,6} = f_{1,4,8} \quad (56)$$

$$f_7 = \frac{1}{2}[\rho_0 - f_0 - 2(f_1 + f_4 + f_8)] \quad (57)$$

$$f_5 = f_7 \quad (58)$$

4.1.2 Temperature field

For temperature field, the general form of LBE is given as:

$$g_i(\vec{x} + \vec{c_i}\delta_t, t + \delta_t) - g_i(\vec{x}, t) = -\frac{1}{\tau_h}\left[g_i(\vec{x}, t) - g_i^{(eq)}(\vec{x}, t)\right] \quad (59)$$

where g_i is distribution function relating to temperature, $g_i^{(eq)}$ is equilibrium distribution function relating to temperature. τ_h is relaxation time relating to temperature, which is obtained as:

$$\tau_h = \frac{3\alpha\delta t}{(\delta x)^2} + \frac{1}{2} \quad (60)$$

$g_i^{(eq)}$ is obtained by (Yan *et al*. 2008):

$$g_i^{(eq)} = T\omega_i\left(1 + \frac{\vec{c_i}\cdot\vec{u}}{c_s^2}\right) \quad (61)$$

Temperature of each discrete point can be calculated as:

$$T = \sum_i g_i \quad (62)$$

The boundary condition of upper and lower wall surface is defined as:

$$T = T_w \quad (63)$$

The boundary condition of the outlet in a fully developed flow state is defined as

$$g_{3,6,7}(n,j) = g_{3,6,7}(n-1,j) \quad (64)$$

The boundary condition of inlet is:

$$T = T_c \quad (65)$$

5. Code validation and grid independence

5.1 Code validation

Poiseuille flow in a channel without porous medium and magnetic field was studied to verify the the present code. And the velocity profile in fully developed regions were

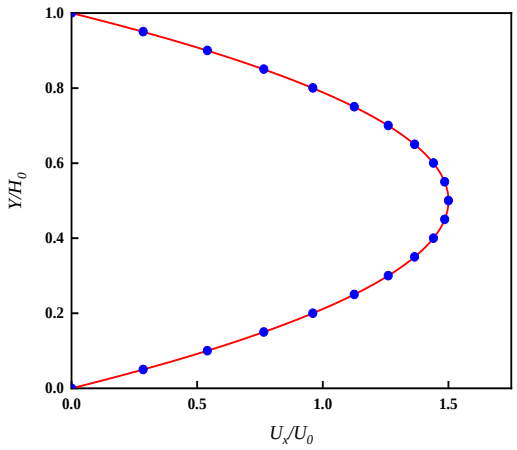

Fig. 3 The velocity profile in fully developed regions: ·, present work; —, analytical result

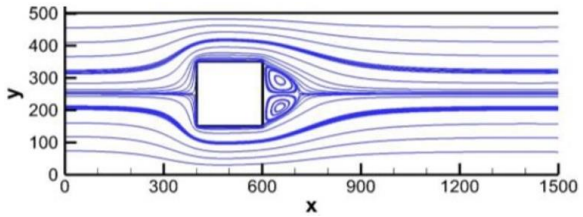

(a) Monireh *et al*. (year) flow field

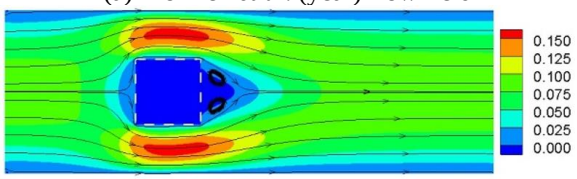

(b) Present work, flow field

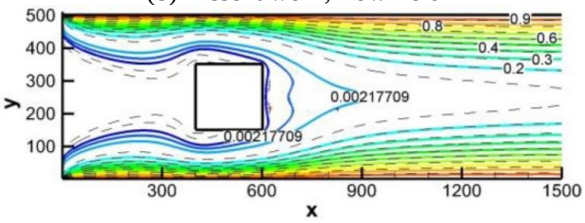

(c) Monireh *et al*. (year) temperature field

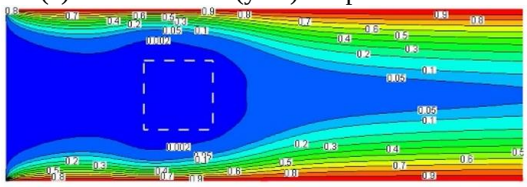

(d) Present work, temperature field

Fig. 4 Calculated flow field and temperature field around the square cylinder in channel

compared with the available analytical result (Salehi *et al*. 2014). It can be found that the numerical result agrees well with the analytical result.

The flow field and temperature field of the flow around the square cylinder in the channel were also simulated and compared with the simulated result of Abchouyeh *et al*. (2018) for further verification. As shown in Fig. 4, the calculated flow field and temperature field for water (no nanoparticles) with the inlet Reynolds number of 100 were found to be consistent with that in the work of Abchouyeh *et al*. (2018).

Table 2 Effect of grid density on the average *Nu* of bottom wall

Grid	300×100	450×150	600×200	750×250
$\overline{Nu}$	7.72	7.68	7.68	7.68
Relative deviation	-	-0.52%	0.00%	0.00%

5.2 Grid independence

To ensure that the calculated result is independent of the number of grids, the grid densities of 300×100, 450×150, 600×200, and 750×250 was used for calculation, respectively. Table 2 shows the average *Nu* of CuO-water nanofluid of Φ=0.02 in zone ① at ε=0.9, *Ha*=100 and θ=90°.

It is clearly that the simulated result no longer changes when the grid density is larger than 450×150. Therefore, a grid density of 450×150 was chosen for calculation.

6. Result and Discussion

6.1 Effect of Ha and ε

Fig. 5 shows the average *Nu* of three nanofluids at the surface of bottom wall against ε at different *Ha*, when Φ is 0.02 and the direction of magnetic field equals 90°. Clearly, it can be found that for all nanofluids, as the porosity decreases, the average *Nu* gradually increases at the same *Ha*. The calculated results show that when *Ha* is 0, the average *Nu* of the CuO-water nanofluids at ε=0.8 is 4.46% larger than that at ε=0.9; for Al_2O_3-water is 4.45%; for Fe_3O_4-water is 4.46%. It indicates that in the case of high-porosity porous medium, porosity variation of porous medium has the same effect on different nanofluids on the heat transfer. This is due to the size of nanoparticles is much smaller than the pore size of porous medium, thus neglecting the size effect of nanoparticles and the effect of nanoparticles being blocked and adsorbed by porous medium, chemical reactions, microscopic forces, and agglomeration.

Fig. 5 also shows that there is a negative correlation between *Nu* and the *Ha*, which indicates that as the magnetic field increases, the heat transfer is inhibited. It is worth noting that different results are found in different studies regarding whether the effect of magnetic fields on the flow and heat transfer of nanofluids is facilitated or inhibited. As mentioned in Section 1, in the studies of Ma *et al*. (2020), Sharif *et al*. (2021a) and Li *et al*. (2019) the magnetic field increases the *Nu*, while in the researches of Farooq *et al*. (2023), Sajjadi *et al*. (2019), Sheikholeslami *et al*. (2019), Rao *et al*. (2023), the magnetic field inhibits the flow and thus inhibits the heat transfer effect. From these researches, it is found that magnetic field increases heat transfer effect generally occurs in natural convection, which

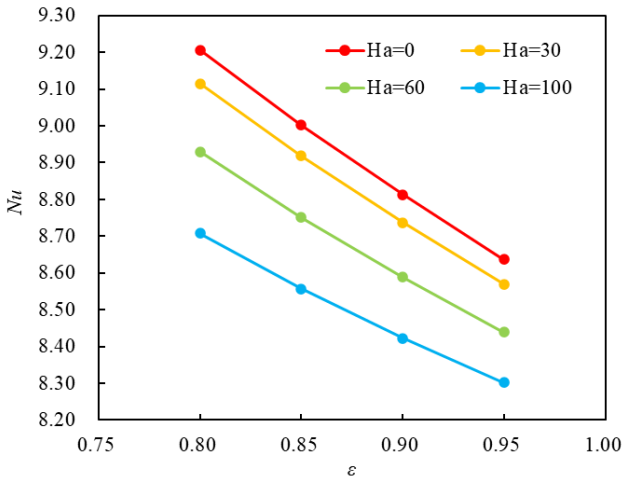

(a) CuO-water

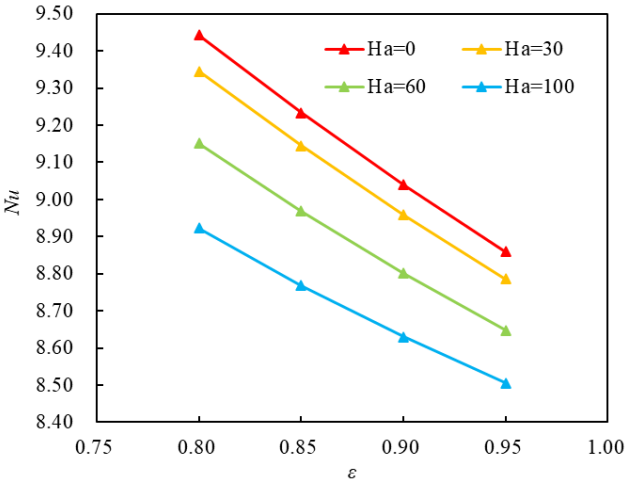

(b) Al_2O_3-water

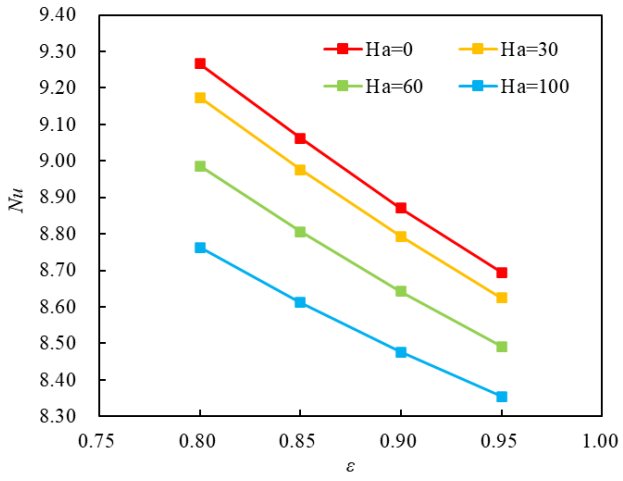

(c) Fe_3O_4-water

Fig. 5 *Nu* as a function of ε at different *Ha* in zone ①

is due to the forces causing convection (e.g., gravity) are not large enough and Lorentz force as the driving force is also a main factor causing convection. At this point, the specifics of the direction of the magnetic field and the area of the calculated *Nu* leads to magnetic field enhancing the local flow and thus enhance convective heat transfer. At the same time, if the concentration variation of the nanofluid is

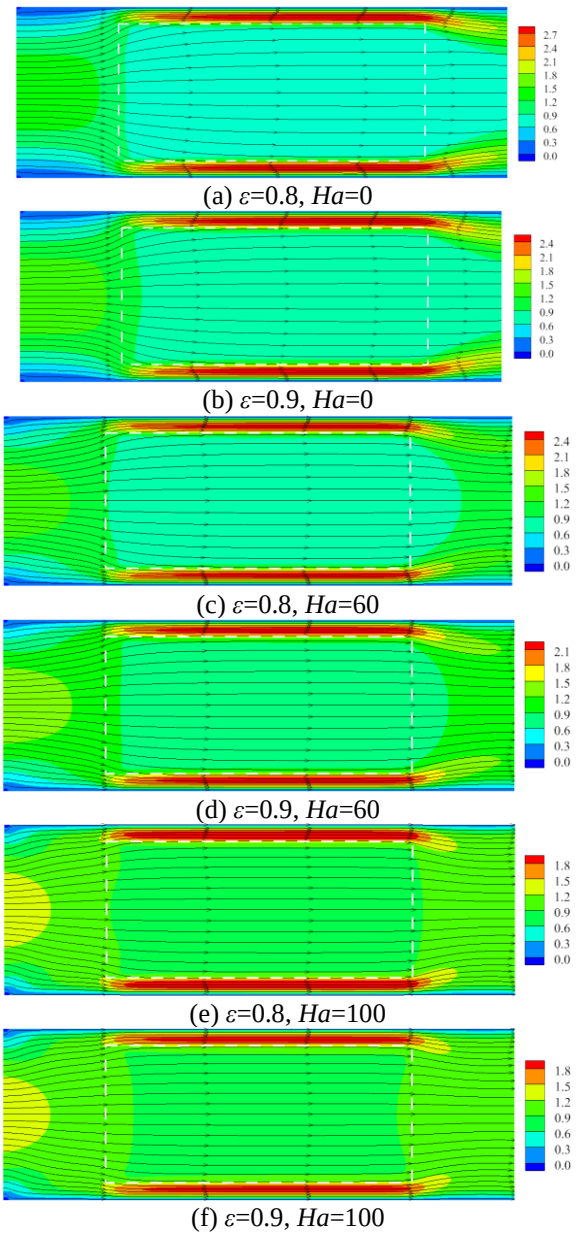

(a) ε=0.8, *Ha*=0

(b) ε=0.9, *Ha*=0

(c) ε=0.8, *Ha*=60

(d) ε=0.9, *Ha*=60

(e) ε=0.8, *Ha*=100

(f) ε=0.9, *Ha*=100

Fig. 6 Flow field distribution of CuO-water nanofluid under different ε and *Ha*

considered, as in the study by Sharif *et al*. (2021a), magnetic field may cause the local concentration of the nanofluid to become larger, thus increasing the thermal conductivity of the local fluid and then enhancing the local heat transfer. While in forced convection, the Lorentz force tends to be smaller compared to the flow driving force, and its effect tends to inhibit the flow in the mainstream direction, causing the calculated local *Nu* to decrease. As shown in Table 3, $\overline{U_x}$ varies with different *Ha*.

As an example, Fig. 6 shows the flow field distribution of CuO-water nanofluid of Φ=0.02 at the direction of magnetic field of 90°. Table 3 shows the relative average flow velocity in zone ① corresponding to the cases in Fig. 6. Fig. 6 and Table 3 show that as the porosity increases, the flow velocity in porous medium zone increases and the flow velocity in zone ① gradually decreases, which means that

Table 3 The relative average flow velocity $\overline{U_x}$ of CuO-water nanofluid in fluid zone adjacent to porous medium under different ε and Ha

	ε	
Ha	0.8	0.9
0	1.96	1.77
60	1.74	1.57
100	1.50	1.37

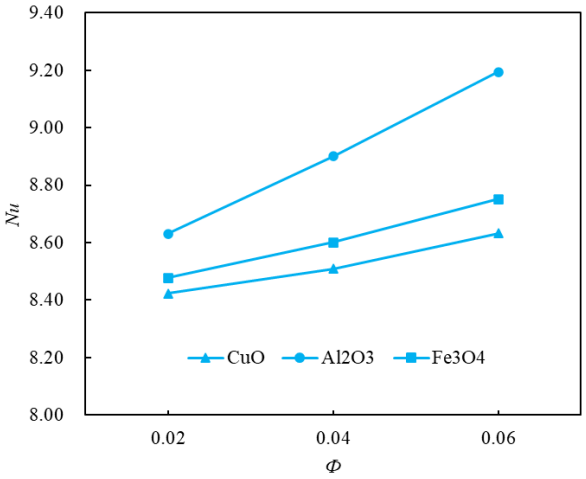

Fig. 7 *Nu* of nanofluids as a function of Φ

the squeezing effect of the porous medium on the fluid is enhanced along with the porosity reduction. Therefore, the porosity reduction of the porous medium can result an improvement on heat exchange. Fig. 6 and Table 3 also show that when the *Ha* increases, the flow velocity in the porous medium increases, indicates that the flow velocity in zone ① decreases. It can be found that the magnetic field enhances the seepage effect of the porous medium, because the magnetic field reduces the velocity flowing into the porous medium, which reduces the resistance of the porous medium to the fluid and reduces the kinetic energy dissipation, refer to Eqs. (27) and (28).

Therefore, it can be briefly summarized that, the reason for the enhanced heat transfer in porous medium is squeezing effect of fluid. Regardless of nanofluid interactions, chemical reactions, adsorption/desorption, squeezing effect is the same for all nanofluids. And promoting or inhibiting effect of the magnetic field on heat transfer depends on the proportion of the Lorentz force contribution to the flow driving force, the direction of the magnetic field and the flow, and the calculated local *Nu* position.

6.2 Effect of Φ and Nanoparticle types

Fig. 7 shows the average *Nu* of the nanofluids of CuO-water, Al_2O_3-water and Fe_3O_4-water with Φ of 0.02, 0.04, and 0.06 at the surface of bottom wall. The conditions of the magnetic field and porous medium are controlled as Ha=100, θ=90°, ε=0.9. It can be learned that the *Nu* of nanofluids increases as the nanoparticle volume-fraction

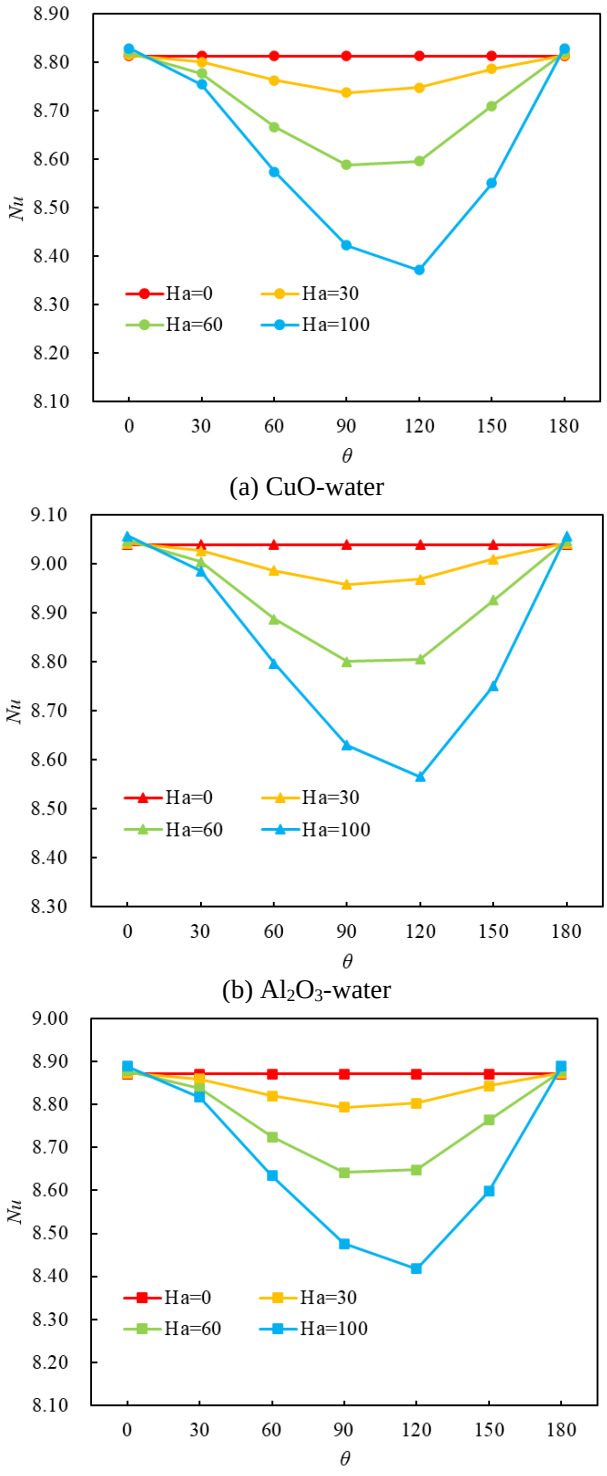

Fig. 8 *Nu* of nanofluids as a function of θ

increases due to higher thermal conductivity, which indicates better heat transfer effect. This is consistent with the conclusions drawn by Chabani *et al.* (2022) and Bouselsal *et al.* (2023). For the three types of nanofluids, due to the bigger thermal conductivity and Prandtl number, the enhancement on the heat transfer effect of Al_2O_3-water nanofluid is more significant than that of the other two nanofluids. At Φ=0.06, *Nu* of Al_2O_3-water is 6.51% larger

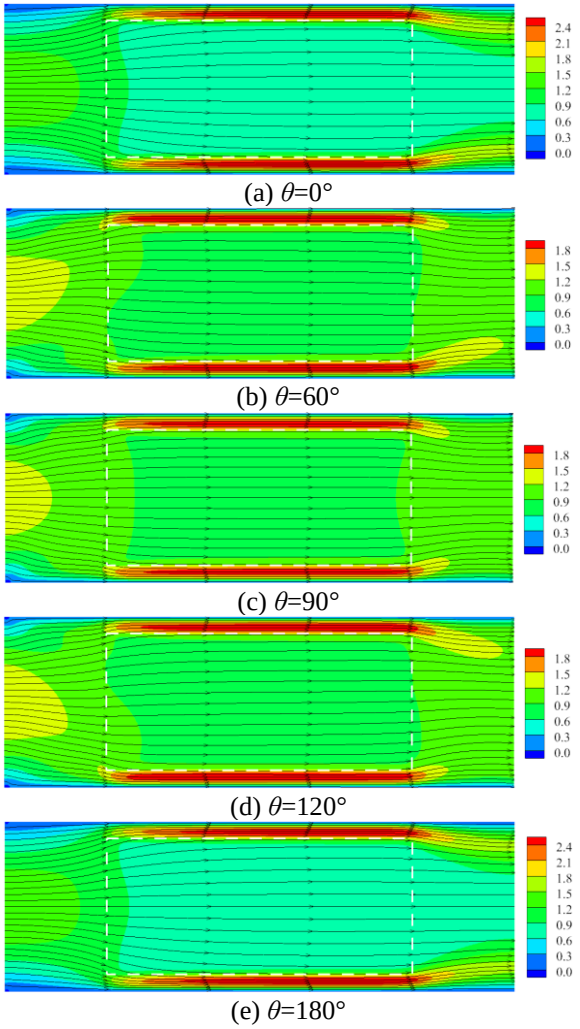

Fig. 9 Flow field of CuO-water nanofluid under different θ at Ha=100

than that of CuO-water and 5.05% larger than that of Fe_3O_4-water. At the same time, it can be seen that changing Al_2O_3 volume-fraction has the most obvious effect on heat transfer. For example, the average Nu for nanofluids with Al_2O_3, Fe_3O_4 and CuO nanoparticles increase by 6.51%, 3.24% and 2.48% respectively, when Φ increases from 0.02 to 0.06.

6.3 Effect of the intensity and direction of magnetic field

The influence of the intensity and direction of the magnetic field on the heat transfer of the three types of nanofluid was simulated, and the results for the case of Φ=0.02 and ε=0.9 are shown in Fig. 8 as an example. It can be clearly found that for the three types of nanofluids, as the intensity increases, the suppression effect of magnetic field on heat transfer becomes greater. In addition, for Ha=30 and Ha=60, the most significant inhibiting effect is at θ=90°; and for Ha=100, the most significant inhibiting effect is at θ=120°. This is because within this θ range, the direction of the magnetic field can be perpendicular to the flow direction as much as possible, thereby maximizing the Lorentz force. It can be seen from the Fig. 8 that when θ=0° or 180°, the direction of the magnetic field is almost parallel to the flow direction, and the Lorentz force has almost no influence. When Ha=100, the direction angle θ with the significant inhibiting effect is larger than when Ha=30 and 60, because a stronger magnetic field intensity will have a greater Lorentz force, resulting in a larger component velocity of the fluid in the y direction, the direction of the combined velocity will be more towards the y direction. If the direction of the magnetic field is to be perpendicular to the flow velocity as much as possible, a larger θ is required.

The flow field of CuO-water nanofluid in Fig.9 indicates that when the magnetic field direction is oblique, the flow field distribution is no longer symmetrical, especially in the fluid zone adjacent to porous medium. At the same time, taking the case of θ=90° as an example, when Ha=100, the average Nu of nanofluids with Al_2O_3, Fe_3O_4 and CuO nanoparticles are reduced by 4.43%, 4.53% and 4.45% respectively, compared with there is no magnetic field. This indicates that due to the paramagnetism of Fe_3O_4, it is more affected by the magnetic field.

7. Conclusions

The magnetohydrodynamics and porous medium were simultaneously used to enhance and control the flow and heat transfer of fluid in rectangular opened channel and their synergistic effect were simulated by using LBM. The following conclusions were obtained:

• Filling the porous medium in the channel can enhance the heat transfer effect due to squeezing effect. As the porosity of the porous medium decreases, the better the heat transfer effect. Regardless of nanofluid interactions, chemical reactions, adsorption/desorption, squeezing effect is the same for all nanofluids.

• Nanofluid can enhance the heat transfer by improving the thermophysical properties of base fluid. The heat transfer effect of the three nanofluids with water as based fluid is in the order of Al_2O_3>Fe_3O_4>CuO. More nanoparticles result better heat transfer effect.

• The magnetic field increases the seepage flow inside the porous medium and reduces the flow in fluid zone adjacent to the porous medium, thereby inhibiting the heat transfer effect on the surface of bottom wall. When Ha=30 and 60, the inhibiting effect is the most significant as the magnetic field angle is 90°. And when Ha=100, the inhibiting effect is the most significant as the magnetic field angle is 120°. Moreover, inhibition of Fe_3O_4-water nanofluid by magnetic field is the most obvious.

• The synergistic effect of nanofluid, porous medium and magnetic field realizes the control of the heat transfer effect.

Acknowledgment

The supports which are provide by the National Natural Science Foundation of China (No. 41941018, No.51936009 and No. 51721004) for the completion of this work are gratefully acknowledged.

References

Abchouyeh, M.A., Mohebbi, R. and Fard, O.S. (2018), "Lattice boltzmann simulation of nanofluid natural convection heat transfer in a channel with a sinusoidal obstacle", *Int. J. Mod. Phys. C.*, **29**(9). https://doi.org/10.1142/S0129183118500791.

Abedini, A., Armaghani, T. and Chamkha, A. J. (2019), "MHD free convection heat transfer of a water–Fe_3O_4 nanofluid in a baffled C-shaped enclosure", *J. Therm. Anal. Calorim.*, **135**(1), 685–695. https://doi.org/10.1007/s10973-018-7225-8.

Babar, H. and Ali, H.M. (2019), "Towards hybrid nanofluids: preparation, thermophysical properties, applications, and challenges", *J. Mol. Liq.*, **281**, 598-633. https://doi.org/10.1016/j.molliq.2019.02.102.

Beriache, M., Sidik, N.A.C., Yazid, M.N.A.W.M., Mamat, R., Najafi, G. and Kefayati, G.H.R. (2016), "A review on why researchers apply external magnetic field on nanofluids", *Int. Commun. Heat Mass Transf.*, **78**, 60-67. https://doi.org/10.1016/j.icheatmasstransfer.2016.08.023.

Boujelbene, M., Rehman, S., Alqahtani, S., Alshehery, S. and Eldin, S.M. (2023), "Thermal transport and magneto-hydrodynamics flow of generalized Newtonian nanofluid with inherent irreversibility between conduit with slip at the walls", *Eng. Appl. Comp. Fluid*, **17**(1), 2182364. https://doi.org/10.1080/19942060.2023.2182364.

Bouselsal, M., Mebarek-Oudina, F., Biswas, N. and Ismail, A.I. (2023), "Heat transfer enhancement using Al_2O_3-MWCNT hybrid-nanofluid inside a tube/shell heat exchanger with different tube shapes", *Micromachines*, **14**, 1072. https://doi.org/10.3390/mi14051072.

Brinkman, H.C. (1952), "The viscosity of concentrated suspensions and solutions", *J. Chem. Phys.*, **20**(4), 571. https://doi.org/10.1063/1.1700493.

Cardellini, A., Fasano, M., Bozorg Bigdeli, M., Chiavazzo, E. and Asinari, P. (2016), "Thermal transport phenomena in nanoparticle suspensions", *J. Phys. Condens. Matter.*, **28**(48). https://doi.org/10.1088/0953-8984/28/48/483003.

Chabani, I., Mebarek-Oudina, F., Vaidya, H. and Ismail, A.I. (2022), "Numerical analysis of magnetic hybrid Nano-fluid natural convective flow in an adjusted porous trapezoidal enclosure", *J. Magn. Magn. Mater.*, **564**, 170142. https://doi.org/10.1016/j.jmmm.2022.170142.

Dai, W.S., Zand, Y., Agdas, A.S., Selmi, A., Roco-Videla, A., Wakil, K. and Issakhov, A. (2021), "The economic and management use of rhododendron petals in potas-sium-ion nano batteries anode via efficient computer simulation", *Adv. Nano Res.*, **10**(6), 503-515. https://doi.org/10.12989/anr.2021.10.6.503.

Darbari, B., Rashidi, S. and Keshmiri, A. (2020), "Nanofluid heat transfer and entropy generation inside a triangular duct equipped with delta winglet vortex generators", *J. Therm. Anal. Calorim.*, **140**(3), 1045-1055. https://doi.org/10.1007/s10973-019-08382-7.

Dong, B., Zhou, X., Zhang, Y., Chen, C. and Li, W. (2018), "Numerical simulation of thermal flow of power-law fluids using lattice boltzmann method on non-orthogonal grids", *Int. J. Heat Mass Transf.*, **126**, 293-305. https://doi.org/10.1016/j.ijheatmasstransfer.2018.05.003.

Ergun, S. (1952), "Fluid flow through packed columns", *Chem. Eng. Prog.*, **48**.

Farooq, U., Akhtar, K., Abbasi, M.M., Hussain, M. and Aldandani, M.(2023), "Convective heat transfer performance of MHD nanofluid flow with temperature dependent viscosity over stretching surface", *Z Angew Math Mech.*, 1-13. https://doi.org/10.1002/zamm.202300053.

Guo, Z. and Zhao, T.S. (2002), "Lattice boltzmann model for incompressible flows through porous media", *Phys. Rev. E*, **66**(3), 1-9. https://doi.org/10.1103/PhysRevE.66.036304.

Guo, Z. and Zheng, C. (2008), "Analysis of lattice boltzmann equation for microscale gas flows: relaxation times, boundary conditions and the knudsen layer", *Int. J. Comut. Fluid Dyn.*, **22**(7), 465-473. https://doi.org/10.1080/10618560802253100.

Guo, Z.L., Zheng C.G., (2008), Theory and Applications of Lattice Boltzmann Method, Science Press, Beijing, China.

Habibzadeh, S., Kazemi-Beydokhti, A., Khodadadi, A. A., Mortazavi, Y., Omanovic, S. and Shariat-Niassar, M. (2010), "Stability and thermal conductivity of nanofluids of tin dioxide synthesized via microwave-induced combustion route", *Chem. Eng. J.*, **156**(2), 471-478. https://doi.org/10.1016/j.cej.2009.11.007.

Hamilton, R. L. (1962), "Thermal conductivity of heterogeneous two-component systems", *Ind. Eng. Chem. Fundam.*, **1**(3), 187-191. https://doi.org/10.1021/i160003a005.

He, Y.L., Wang Y., Li Q. (2008), *Lattice Boltzmann Method: Theory and Applications*, Science Press, Beijing, China.

Iqbal, W., Jalil, M., Qazaq, A., Khadimallah, M.A., Naeem, M.N., Hussain, M., Mahmoud, S.R., Ghandourah, E. and Tounsi, A. (2021), "Effect of suction on flow of dusty fluid along exponentially stretching cylinder", *Adv. Nano Res.*, **10**(3), 263-270. https://doi.org/10.12989/anr.2021.10.3.263.

Izadi, M., Hoghoughi, G., Mohebbi, R. and Sheremet, M. (2018), "Nanoparticle migration and natural convection heat transfer of Cu-water nanofluid inside a porous undulant-wall enclosure using LTNE and two-phase model", *J. Mol. Liq.*, **261**, 357-372. https://doi.org/10.1016/j.molliq.2018.04.063.

Kadhim, H.T., Dulaimi, Z.M.A. and Rona, A. (2023), "Local thermal non-equilibrium analysis of Cu-Al_2O_3 hybrid nanofluid natural convection in a partially layered porous enclosure with wavy walls", *J. Appl. Comput. Mech.*, **9**(3), 712-727. https://doi.org/ 10.22055/jacm.2022.42046.3863.

Kang, X., Liao, Q., Zhu, X. and Yang, Y. (2010), "Non-equilibrium extrapolation method in the lattice boltzmann simulations of flows with curved boundaries (non-equilibrium extrapolation of LBM)", *Appl. Therm. Eng.*, **30**(13), 1790-1796. https://doi.org/10.1016/j.applthermaleng.2010.03.032.

Khan, M.I., Khan, W.A., Waqas, M., Kadry, S., Chu, Y.M. and Ali, Z. (2020), "Numerical simulation for MHD Darcy-Forchheimer three-dimensional stagnation point flow by a rotating disk with activation energy and partial slip", *Appl. Nanosci.*, **10**, 5469-5477. https://doi.org/10.1007/s13204-020-01517-5.

Khan, U., Mebarek-Oudina, F., Zaib, A., Ishak, A., Bakar, S.A., Sherif, E.S.M. and Baleanu, D. (2022), "An exact solution of a Casson fluid flow induced by dust particles with hybrid nanofluid over a stretching sheet subject to Lorentz forces", *Wave Random Complex*, 1-14. https://doi.org/10.1080/17455030.2022.2102689.

Li, Z., Sheikholeslami, M., Mittal, A. S., Shafee, A. and Haq, R. (2019), "Nanofluid heat transfer in a porous duct in the presence of Lorentz forces using the lattice boltzmann method", *Eur. Phys. J. Plus.*, **134**(1). https://doi.org/10.1140/epjp/i2019-12406-8.

Ma, Y., Mohebbi, R., Rashidi, M.M., Yang, Z. and Sheremet, M. (2020), "Nanoliquid thermal convection in I-shaped multiple-pipe heat exchanger under magnetic field influence", *Phys. A*, **550**, 124028. https://doi.org/10.1016/j.physa.2019.124028.

Manna, N.K., Mondal, M.K. and Biswas, N. (2021), "A novel multi-banding application of magnetic field to convective transport system filled with porous medium and hybrid nanofluid", *Phys. Scr.* **96**. https://doi.org/10.1088/1402-4896/abecbf.

Mebarek-Oudina, F. (2018), "Convective heat transfer of Titania nanofluids of different base fluids in cylindrical annulus with discrete heat source", *Heat Transf. Asian Res.*, 1-13.

https://doi.org/10.1002/htj.21375.
Mebarek-Oudina, F., Chabani, I. (2022), "Review on nano-fluids applications and heat transfer enhancement techniques in different enclosures", *J. Nanofluids*, **11**, 155-168. https://doi.org/10.1166/jon.2022.1834.
Mebarek-Oudina, F., Preeti, Sabu, A.S., Vaidya, H., Lewis, R.W., Areekara, S., Mathew, A. and Ismail A.I. (2023), "Hydromagnetic flow of magnetite-water nanofluid utilizing adapted Buongiorno model", *Int. J. Mod. Phys. B*, 2450003. https://doi.org/10.1142/S0217979224500036.
Mohamad, A.A. (2015), *Lattice Boltzmann Method: Fundamentals and Engineering Applications with Computer Codes*, Publishing House of Electronics Industry, Beijing, China.
Mondal, S., Dey, A. and Pal, U. (2016), "Low temperature wet-chemical synthesis of spherical hydroxyapatite nanoparticles and their in situ cytotoxicity study", *Adv. Nano Res.*, **4**(4), 295-307. https://doi.org/10.12989/anr.2016.4.4.295.
Murali Krishna, V. and Sandeep Kumar, M. (2019), "Numerical analysis of forced convective heat transfer of nanofluids in microchannel for cooling electronic equipment", *Mater. Today Proc.*, **17**, 295-302. https://doi.org/10.1016/j.matpr.2019.06.433.
Nfawa, S.R., Abu Talib, A.R., Basri, A.A. and Masuri, S.U. (2021), "Novel use of MgO nanoparticle additive for enhancing the thermal conductivity of CuO/Water nanofluid", *Case Stud. Therm. Eng.*, **27**(6), 101279. https://doi.org/10.1016/j.csite.2021.101279.
Patel, H.E., Das, S.K., Sundararajan, T., Sreekumaran Nair, A., George, B. and Pradeep, T. (2003), "Thermal conductivities of naked and monolayer protected metal nanoparticle based nanofluids: manifestation of anomalous enhancement and chemical effects", *Appl. Phys. Lett.*, **83**(14), 2931-2933. https://doi.org/10.1063/1.1602578.
Ramesh, K., Mebarek-Oudina, F., Ismail, A.I., Jaiswal, B.R., Warke, A.S., Lodhi, R.K. and Sharma, T. (2023), "Computational analysis of radiative non-Newtonian Carreau nanofluid flow in a microchannel under the magnetic properties", *Sci. Iran. B.*, **30**(2), 376-390. https://doi.org/10.24200/sci.2022.58629.5822.
Rao, S. and Deka, P.N. (2023), "A study on MHD flow of SWCNT-Al_2O_3/water hybrid nanofluid past a vertical permeable cone under the influence of thermal radiation and chemical reactions", *Numer. Heat Transf. A*, 1-21. https://doi.org/10.1080/10407782.2023.2207731.
Raza, J., Mebarek-Oudina, F. and Lund, L.A. (2022), "The flow of magnetised convective Casson liquid via a porous channel with shrinking and stationary walls", *Pramana J. Phys.*, **96**(4), 1-10. https://doi.org/10.1007/s12043-022-02465-1.
Sajjadi, H., Amiri Delouei, A., Izadi, M. and Mohebbi, R. (2018), "Investigation of MHD natural convection in a porous media by double MRT lattice boltzmann method utilizing MWCNT-Fe_3O_4/water hybrid nanofluid", *Int. J. Heat Mass Transf.*, **132**, 1087-1104. https://doi.org/10.1016/j.ijheatmasstransfer.2018.12.060.
Salehi, A., Abbassi, A. and Nazari, M. (2014), "Numerical solution of fluid flow and conjugate heat transfer in a channel filled with fibrous porous media - a lattice boltzmann method approach", *J. Porous Media.*, **17**(12), 1075-1091. https://doi.org/10.1615/JPorMedia.v17.i12.50.
Sharif, H., Khadimallah, M.A., Naeem, M.N., Hussain, M., Hussain, S. and Tounsi, A. (2021), "Flow of MHD Powell-Eyring nanofluid: Heat absorption and Cattaneo-Christov heat flux model", *Adv. Nano Res.*, **10**(3), 221-234. https://doi.org/10.12989/anr.2021.10.3.221.
Shafiq, A., Mebarek-Oudina, F., Sindhu, T.N. and Rasool, G. (2022), "Sensitivity analysis for Walters-B nanoliquid flow over a radiative Riga surface by RSM", *Sci. Iran. B*, **29** (3), 1236-1249. https://doi.org/10.24200/sci.2021.58293.5662.
Sheikholeslami, M. and Ganji, D.D. (2016), "Nanofluid convective heat transfer using semi analytical and numerical approaches: a review", *J. Taiwan Inst. Chem. Eng.*, **65**, 43-77. https://doi.org/10.1016/j.jtice.2016.05.014.
Sheikholeslami, M., Gorji-Bandpy, M. and Ganji, D.D. (2014), "MHD free convection in an eccentric semi-annulus filled with nanofluid", *J. Taiwan Inst. Chem. Eng.*, **45**(4), 1204-1216. http://dx.doi.org/10.1016/j.jtice.2014.03.010.
Sheikholeslami, M., Keramati, H., Shafee, A., Li, Z., Alawad, O.A. and Tlili, I. (2019), "Nanofluid MHD forced convection heat transfer around the elliptic obstacle inside a permeable lid drive 3D enclosure considering lattice boltzmann method", *Phys. A*, **523**, 87-104, https://doi.org/10.1016/j.physa.2019.02.014.
Singh, S.P., Verma, A.K., Jaiswal, A.K., Singh, D. and Yadav, R.R. (2021), "Study of ultrasonic and thermal properties for heat transfer enhancement in Fe_2O_3 nanoparticles-ethylene glycol nanofluids", *Int. J. Thermophys.*, **42**(4), 1-17. https://doi.org/10.1007/s10765-021-02809-w.
Yan, Y.Y. and Zu, Y.Q. (2008), "Numerical simulation of heat transfer and fluid flow past a rotating isothermal cylinder - a LBM approach", *Int. J. Heat Mass Transf.*, **51**(9-10), 2519-2536. https://doi.org/10.1016/j.ijheatmasstransfer.2007.07.053.
Yu, W. and Choi, S.U.S. (2004), "The role of interfacial layers in the enhanced thermal conductivity of nanofluids: a renovated Hamilton-Crosser model", *J. Nanopart. Res.*, **6**(4), 355-361. https://doi.org/10.1007/s11051-004-2601-7.
Yusoff, A.H.M., Salimi, M.N. and Jamlos, M.F. (2018), "A review: Synthetic strategy control of magnetite nanoparticles production", *Adv. Nano Res.*, **6**(1), 1-19. https://doi.org/10.12989/anr.2018.6.1.001.

CC